RSC Advances

ROYAL SOCIETY OF CHEMISTRY

www.rsc.org/advances

An ABA triblock containing a central soft block of poly[2,5-di(*n*-hexogycarbonyl)styrene] and outer hard block of poly(4-vinylpyridine): synthesis, phase behavior and mechanical enhancement

Xin Liu,[†] Rui-Ying Zhao,[†] Ti-Peng Zhao,[‡] Chen-Yang Liu,[‡] Shuang Yang[†,*] and Er-Qiang Chen[†,*]

[†] *Beijing National Laboratory for Molecular Sciences, Key Laboratory of Polymer Chemistry and Physics of the Ministry of Education, College of Chemistry and Molecular Engineering, Peking University, Beijing 100871, China. E-mail: shuangyang@pku.edu.cn; eqchen@pku.edu.cn.*

[‡] *Beijing National Laboratory for Molecular Sciences, CAS Key Laboratory of Engineering Plastics, Joint Laboratory of Polymer Science and Materials, Institute of Chemistry, The Chinese Academy of Sciences, Beijing 100190, China*

ABSTRACT: We designed and synthesized a series of ABA triblock copolymers containing inner soft poly[2,5-di(*n*-hexogycarbonyl)styrene] (PHCS) block and outer hard poly(4-vinylpyridine) (P4VP) block, wherein the PHCS block has the potential to form a columnar liquid crystalline phase at high temperatures and the P4VP block can complex with metal salt or organic molecules via non-covalent interactions. Using atom transfer radical polymerization method, we prepared successfully the triblock samples with controlled molecular weights and compositions. The triblocks were characterized with various experimental techniques including differential scanning calorimetry, dynamic mechanical analysis, small-angle X-ray scattering, and transmission electron microscopy. The experimental results indicate the occurrence of microphase separation. With the P4VP volume fraction lower than 20%, the triblocks exhibit the phase morphologies of cylindrical or spherical hard P4VP domains arranged in the

soft PHCS matrix. Mechanical property test reveals that the tensile strength and maximum elongation at break can be tuned by varying the total MW and composition of the samples, indicating that the triblock copolymer can be used as thermoplastic elastomer while carrying functional blocks. Applying the metal-ligand coordination interaction between P4VP and Zn^{2+}, we prepared the hybrid of triblock and zinc perchlorate. Domain spacing expansion and phase morphology change induced by adding the metal salt are detected. Furthermore, because of the hybrid formation and the glass transition temperature of hard phase increased dramatically by adding only a small amount of the salt, rubbery plateau of the hybrid is extended, indicating a better thermal stability than that of the pure triblock.

Introduction

Microphase separation of block copolymers at a length scale ranging from 5 to 100 nm furnishes access to a variety of functional and technologically useful materials. In order to tune the bulk materials' properties, control over the morphologies and stabilities of the microphase separated structures is achieved by rational designing the size, shape, and interactions of their constituents.[1-4] Coil-coil diblock copolymers can self-assemble into phase morphologies of lamellae, hexagonally packed cylinders, bicontinuous gyroids, or body-centered cubic spheres.[5,6] ABA triblocks can also have the similar microphase separated structures. On the other hand, as both ends of the B block can be constrained to the A/B interfaces, ABA triblock is obviously distinct from AB diblocks. Presence of the bridges linking separated interfaces together strongly affects the mechanical properties of the triblock-based materials.[7] Because they can possess both elastomeric and thermoplastic features due to the microphase-separated structures, triblock copolymers have gained widely investigation.[8-10] Containing a soft central block of B and the two hard blocks of A, the triblock copolymer such as polystyrene-*b*-polybutadiene-*b*-polystyrene (SBS) is a typical thermoplastic elastomer (TPE).[11,12] The relationship between the microphase separation behaviors and the mechanical properties of triblock copolymers has been intensely studied by changing the segment fraction[13] or the segment-segment interaction energy.[14]

Modern synthetic chemistry including anionic polymerization,[15] ring-opening metathesis polymerization,[16] nitroxide-mediated polymerization,[17] reversible addition-fragmentation transfer[18] or atom transfer radical polymerization (ATRP)[19] enables to tailor the chemical structures, and hence the properties of well-defined ABA triblocks. The TPE triblock copolymers consisting of various constituents now can be prepared in a facile synthetic way. For instances, the candidates for the hard segments can be poly(methyl methacrylate),[20] polyacrylonitrile,[21] poly(α-methylene-g-butyrolactone),[22,23] poly[4-(1-adamantyl)styrene];[24] and for the soft segments, poly(1,4-polyisoprene),[24]

poly(*n*-butyl acrylate)[18,19,25] can be used. In the new molecular design and synthesis of TPE, one main target is to increase the glass transition temperature (T_g) of the hard segment and improve the chemical stability of the soft segment.[18,19,21,24-26] Moreover, it is also of interest to equip the triblock with some particular functionality. For example, one option towards this aim is introducing liquid crystal (LC) property to the ABA triblock copolymers. Gronski et al. first proposed the concept of thermoplastic liquid crystalline triblock elastomers by attaching mesogenic units onto the PB backbone of SBS.[27] Zhao et al. prepared a similar LC TPE by grafting LC acrylic polymer onto the central PB backbone of SBS.[28,29] The triblock with LC/isotropic/LC sequence was also obtained with the end blocks being an azobenzene-containing side-chain LC polymer and the midblock a rubbery polymer,[30] which coupled LC phase formation and photoisomerization of the azobenzene chromophore together. Another ABA type triblock with LC/isotropic/LC sequence was reported by Yi, Y. et al., which consisted of poly{2,5-bis[(4-methoxyphenyl)oxycarbonyl]styrene} (PMPCS) as the hard A block and poly(*n*-butyl acrylate) as the soft B block.[31] PMPCS is a typical mesogen-jacketed liquid crystalline polymer (MJLCP), with the mesogenic pendants laterally attached to the polyethylene backbones through a single carbon-carbon bond. The whole MJLCP chain backbone is largely stretched due to the steric hindrance imparted by the densely packed mesogenic side-groups.[32,33] Incorporation of liquid crystallinity to the hard domains which serves as "physical cross-links" may enhance the microphase separation and improve the stability above T_g due to the formation of LC phase.[31,34]

Here, we report a new ABA type triblock copolymer with poly[2,5-di(*n*-hexogycarbonyl)styrene] (PHCS) as the soft B block and poly(4-vinylpyridine) (P4VP) as the hard A block, of which the molecular design is shown in Scheme 1. According to the molecular structure, one can notice that PHCS bears some similarity to PMPCS, wherein the side groups belong to terephthalate. In our previous study, we have found that the terephthalate side-group of PHCS can in fact impose "jacketing" effect strong

enough on the polyethylene backbone, resulting in a long-range ordered hexagonal columnar (Φ_H) phase at high temperatures.[35,36] On the other hand, the Φ_H phase will disappear upon cooling, and PHCS becomes amorphous at low temperatures (e.g., at room temperature). In this case, PHCS renders a sort of "isotropic re-entrant" behavior.[35-37] It is also worthy to note that the homo-PHCS possesses a T_g around -30 °C, far below the room temperature. Therefore, we consider that PHCS can act as the soft segment for an ABA triblock copolymer with the TPE characteristics (see Scheme 1). Assuming that the PHCS block exhibits the "isotropic re-entrant" behavior, heating the PHCS containing ABA triblock may lead to the Φ_H phase formation which may enhance the mechanical properties of the triblock. Moreover, the Φ_H phase of PHCS is characterized by the parallel packing of cylinder-like chains. It is also interesting to see whether stretching of the ABA triblock specimens can change the conformation of the PHCS blocks from coil to extended and thus result in the Φ_H phase.

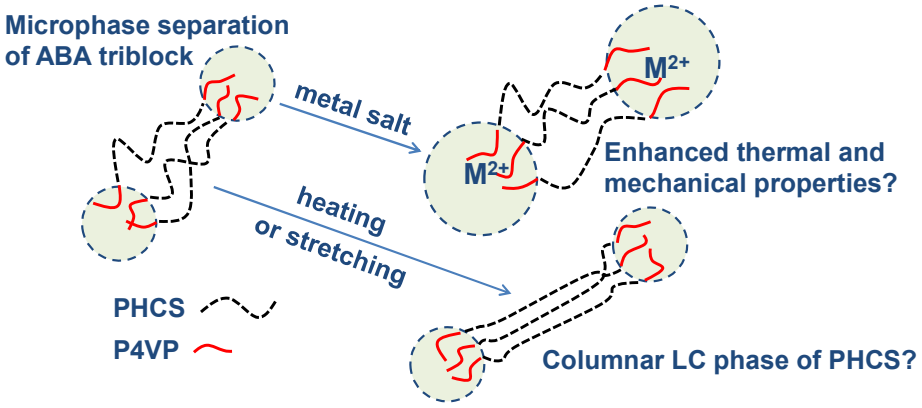

Scheme 1 Molecular design of P4VP-*b*-PHCS-*b*-P4VP.

For the triblock we synthesized, P4VP is selected to substitute the commonly used polystyrene (PS) as the hard segment. It has been demonstrated that block copolymers containing P4VP with polar group of pyridine on every repeating unit has the ability to form various self-assembly structure.[38-40] Moreover, the multiple interaction sites of P4VP offer the location to complex with metal salts or organic molecules, providing a facile way to tune the phase behavior and mechanical property.[41-43] Block copolymer/metal salt hybrids via metal-to-ligand coordination exhibit clear microphase-separated

structures composed of an organic phase and a hybrid phase containing metal salts. They combine the flexibility and processability of organic materials and the useful features of inorganic materials.[44-46] By introducing the metal salt into our triblock copolymer, our goal is to prepare the functional triblock copolymer with tunable phase morphology while improving the thermal and mechanical properties (see Scheme 1).

In this paper, we describe the synthesis of P4VP-*b*-PHCS-*b*-P4VP with different molecular weights (MWs) and compositions using ATRP method. We studied the microphase separation of the triblock using various techniques including thermal analysis, small-angle X-ray scattering (SAXS), and transmission electron microcopy (TEM). The results show that the triblock copolymers with the P4VP volume fraction less than 20% can self-assemble into the cylindrical or spherical morphologies with the PHCS block as the continuous phase. The strong microphase separation ensures the triblock to have stable mechanical property. Moreover, we prepared the hybrid of the triblock copolymer with zinc perchlorate. The metal salt coordinated to the P4VP block influences the phase behavior significantly. Adding a small amount of the salt can have a positive impact on the mechanical property.

Experimental

Materials. 4-vinylpyridine (4VP) (Alfa Aesar, 98%) and N,N-dimethylformamide (DMF, Beijing Chemical Reagents Co., A.R.) were distilled from CaH_2 under reduced pressure before use. Chlorobenzene (Beijing Chemical Reagents Co., A.R.) was purified by washing with concentrated sulfuric acid to remove residual thiophenes, followed by washing with deionized water, a 3% sodium carbonate solution and with deionized water again, and then dried with anhydrous calcium chloride before it was finally distilled. Tetrahydrofuran (THF, Beijing Chemical Reagents Co., A.R.), dichloromethane (CH_2Cl_2, Beijing Chemical Reagents Co., A.R.), and 2-propanol (Beijing Chemical

Reagents Co., A.R.) were used after distilled. N,N,N',N",N"-pentamethyldiethylenetriamine (PMDETA, TCI, 98%), tris(N,N,-dimethylamino)ethyl)amine (Me_6TREN, Alfa Aesar, 98%), Cu(I)Cl (Alfa Aesar, 99%), and diethyl-meso-2,5-dibromoadipate (Alfa Aesar, 98%), Zinc(II) perchlorate ($Zn(ClO_4)_2$, Heowns, 98%) were used as received. Vinyl terephthalic acid was synthesized according to the literature.[33] Synthesis and characterization of the monomer 2,5-di(*n*-hexogycarbonyl)styrene (HCS) were described in Scheme S1 of Supporting Information.

Instruments. ^{1}H NMR (400 MHz) spectra were recorded on a Bruker ARX400 spectrometer at room temperature using $CDCl_3$ or CD_2Cl_2 as the solvent. Elemental analysis was performed with an ElementarVario EL instrument. Gel permeation chromatography (GPC) was conducted on a Waters 2410 instrument equipped with 2410 refractive-index detector at 35 °C. THF was used as the eluent at a flow rate of 1.0 ml min^{-1}. The GPC calibration curve was obtained with linear PS standards. Using a series of THF solutions (1.0~5.0 mg/mL), the specific refractive index increment (d*n*/d*c*) of PHCS in THF was measured by a Wyatt Optilab T-rEX equipped with a 600 nm laser. With the d*n*/d*c* value of 0.115 ml g^{-1}, the absolute MW of PHCS was determined using a LS-GPC (Wyatt Technology DAWN HELEOS) with THF as the eluent.

Differential scanning calorimetry (DSC) measurements were carried out on a TA Q100 DSC calorimeter in a nitrogen atmosphere. The samples with a typical weight of ~8 mg were encapsulated in hermetically sealed aluminum pans. For the triblock, the temperature range of DSC experiments was from -80 to 170 °C. Thermogravimetric analysis (TGA) was performed on a Q600 instrument.

SAXS experiments were carried out on an Anton Paar SAXSess using Cu Kα radiation as the X-ray source. The scattering patterns were recorded on an imaging-plate covering the *q*-range from 0.06 to 29 nm^{-1} ($q = 4\pi\sin\theta/\lambda$, where λ is the X-ray wavelength of 0.154 nm and 2θ the scattering angle). The scattering peak positions were calibrated with silver behenate. TEM bright-field images were obtained

using a T20 TEM operating at an accelerating voltage of 120 kV. Ultramicrotome was used to prepare the microtomed samples. Thin sections of ~50 nm were collected on TEM copper grids, followed by staining in RuO_4 vapor for approximately 15 min.

Tensile property measurements were conducted at 25 °C with TA ARES-G2 rheometer utilizing its solid tensile fixture that gripped a dumbbell-shaped specimen. The dumbbell-shaped samples with the width of 4 mm and thickness of ~0.5 – 1.0 mm were drawn with the rate of 0.6 mm s^{-1} at room temperature. Dependencies of stress versus strain ratio were recorded. Elongation at break, and stress at break were determined by averaging the results of 2-3 independent drawing experiments performed at the same conditions.

Dynamic mechanical analysis (DMA) was conducted on a TA Instruments Q800 Dynamic Mechanical Analyzer. The samples were prepared in a rectangular mold (the sample dimension: 23 mm×4.5 mm×1 mm). The thermal DMA experiments were carried out from -80 to 275 °C at a heating rate of 3 °C min^{-1} using a tension film clamp keeping a constant frequency of 1 Hz and oscillating amplitude of 20 μm.

Synthesis of difunctional macroinitiator Cl-PHCS-Cl. Diethyl-meso-2,5-dibromoadipate (8 mg, 0.022 mmol), PMDETA (8.9 μL, 0.045 mmol), and 2,5-di(*n*-hexogycarbonyl)styrene (1.6 g, 4.44 mmol), chlorobenzene (2.4 g) were successively introduced into a 20 mL reaction tube. After one freeze-pump-thaw cycle, the tube was filled with nitrogen and CuCl (2.22 mg, 0.022 mmol) was quickly added to the frozen mixture. After other three freeze-pump-thaw cycles, the tube was sealed under vacuum and inserted into an oil bath at 90 °C. A typical ratio of monomer : initiator : catalyst : ligand applied was 200:1:1:2. The polymerization process was stopped after 3.5 h, and then THF was added to the reaction mixture. The resultant polymer solution was purified by passing through a neutral alumina column to remove the residual copper salts. Then, the polymer solution was concentrated and precipitated into cold

methanol for three times. The precipitate was collected and then dried in vacuum for 24 h at 40 °C. Yield: 50%. ^{1}H NMR ($CDCl_3$, 400 MHz), δ (ppm): 7.0-8.0 (s, 3H, in phenyl ring), 3.0-4.0 (m, 4H, COOCH_2CH$_2$), 1.5-2.0 (s, 1H, CHCH$_2$), 1.5-2.0 (s, 2H, CHCH_2), 1.0-1.5 (s, 16H, COOCH$_2$CH_2), 0.5-0.9 (s, 6H, CH$_2$CH_3).

Synthesis of triblock copolymer P4VP-*b*-PHCS-*b*-P4VP. The triblock samples with different block length were prepared based on using a different feed ratio of the macroinitiator Cl-PHCS-Cl and 4VP. In a typical experiment, Cl-PHCS-Cl (1.146 g, 0.026 mmol) was dissolved in 5 mL of mixed dry chlorobenzene/2-propanol (6/4) and added into polymerization tube containing 4VP (0.458 g, 4.36 mmol) and Me_6TREN (12.9 μL, 0.044 mmol). After one freeze-pump-thaw cycle, the tube was filled with nitrogen, and CuCl (2.2 mg, 0.022 mmol) was quickly added to the frozen mixture. After other three freeze-pump-thaw cycles, the tube was sealed under vacuum and inserted into an oil bath at 40 °C. The solution turned yellow and viscous. After 7 h, the polymerization process was stopped. Then, THF (about 50 mL) was added to the reaction mixture. The mixture was then filtered through a column of alumina to remove the residual copper salts. The volume of the solution was reduced to approximately 5 mL, and the solution was precipitated into a 10-fold excess of diethyl ether. The polymer was isolated and redissolved in THF (5 mL), and the precipitation cycle was repeated several times to remove the unreacted 4VP and macroinitiator Cl-PHCS-Cl since PHCS has a good solubility in diethyl ether. Then the resultant polymer was dried under vacuum for 12 h. Yield: 60%. ^{1}H NMR ($CDCl_3$, 400 MHz), δ (ppm): 8.0-9.0 (s, 2H, in pyridine ring), 7.0-8.0 (s, 3H, in phenyl ring), 6.0-7.0 (s, 2H, in pyridine ring), 3.0 to 4.0 (m, 4H, COOCH_2CH$_2$), 1.5-2.0 (s, 1H, CHCH$_2$), 1.5-2.0 (s, 2H, CHCH_2), 1.0-1.5 (s, 16H, COOCH$_2$CH_2), 0.5-0.9 (s, 6H, CH$_2$CH_3).

Preparation of triblock/metal salt hybrids. The hybrids of triblock/metal salt were prepared by a solution-casting method. $Zn(ClO_4)_2$ was used as a readily available metal salt. Chloroform and

acetonitrile, which are good solvents for P4VP-*b*-PHCS-*b*-P4VP and $Zn(ClO_4)_2$, were used as solvents to ensure the homogenous complexation based on the metal-to-ligand coordination interaction between Zn^{2+} and pyridine groups. In a typical procedure, P4VP-*b*-PHCS-*b*-P4VP solution in chloroform and a $Zn(ClO_4)_2$ solution in acetonitrile solution were prepared separately, and then these two were blended together with a desired mole ratio of Zn^{2+} to 4VP ($[Zn^{2+}]/[4VP]$). After stirring for 12 h, the blending solution was cast onto the Teflon plate. The obtained solution-cast film was dried for 72 h in vacuum at room temperature.

Results and Discussion

Synthesis of P4VP-*b*-PHCS-*b*-P4VP. To synthesize the triblock of P4VP-*b*-PHCS-*b*-P4VP, two steps were taken as shown in Scheme 2. First, the difunctional macroinitiator Cl-PHCS-Cl was synthesized via ATRP at 90 °C using CuCl/PMDETA as the catalyst and diethyl-meso-2,5-dibromoadipate as the difunctional initiator. CuCl was used as the Cu(I) species to invoke the halogen exchange and to enhance the rate of initiation over the rate of propagation. Molecular characterization data of the obtained Cl-PHCS-Cl were given in Table SI-1 in Supporting Information. Since the resonance peaks of the protons at the chain center which belong to the ATRP difunctional initiator and the protons at the chain ends of the Cl-PHCS-Cl overlap with that of PHCS, the MW of the macroinitiator cannot be determined by ^{1}H NMR. In this case, LS-GPC was employed to obtain the absolute MW. For the Cl-PHCS-Cl samples, the number average MWs (M_ns) by LS-GPC are ranged from 18 to 57 kg mol^{-1}, 1.40~1.60 times larger than that obtained by GPC calibrated with PS standards, and the polydispersities (PDIs) are of around 1.25.

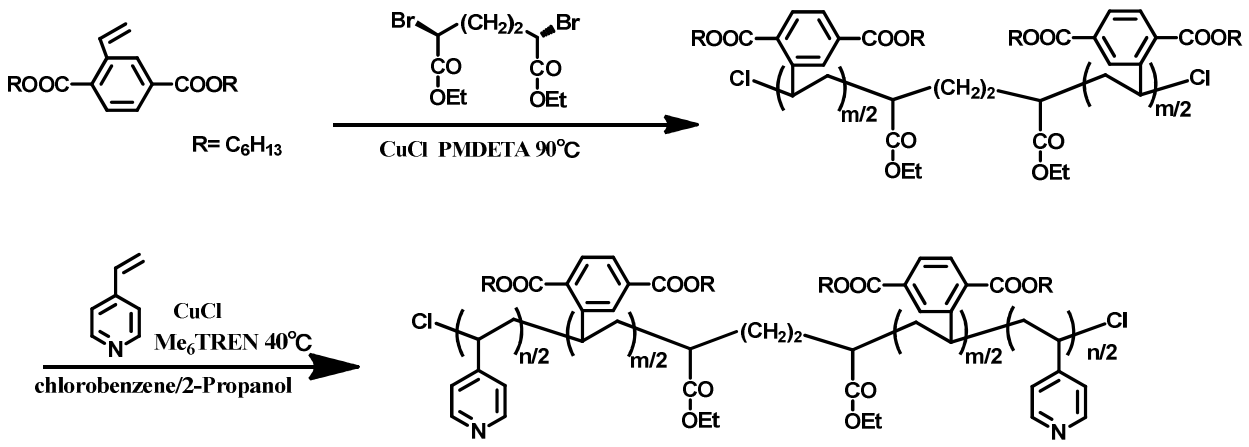

Scheme 2 Synthetic route of the macroinitiator Cl-PHCS-Cl and the triblock P4VP-*b*-PHCS-*b*-P4VP.

In the second step of synthesis, the triblock copolymer was prepared by ATRP method with Cl-PHCS-Cl as the macroinitiator. Controlled polymerization and incorporation of P4VP into block copolymers based on ATRP method is challenging, because the strong coordination pyridine could compete for the binding with the metal catalysts in these systems.[47,48] Pyridine-coordinated copper complex will significantly slow down the polymerization rate, leading to a low yield. Therefore, a much stronger ligand Me_6TREN rather than the common ATRP ligand of PMDETA was introduced into the system to compete with 4VP monomer. For the 4VP polymerization, a protic solvent is necessary. However, the macroinitiator of Cl-PHCS-Cl cannot be dissolved in the protic solvent such as 2-propanol. In this case, we used a mixed solvent of chlorobenzene and 2-propanol as the reaction media. Using Br as the halogen and CuBr/Me_6TREN as the catalyst could result in an amount of termination reactions,[49,50] and thus the chlorine-based macroinitiator is required. During polymerization of 4VP, the strong C-Cl bond balances the activation/deactivation by the CuCl/Me_6TREN complex for a suitable concentration of the active radicals. To ensure the end reactivity and higher initiator efficiency, the conversion should be controlled in a relatively low range (i.e., conversion lower than 50%).

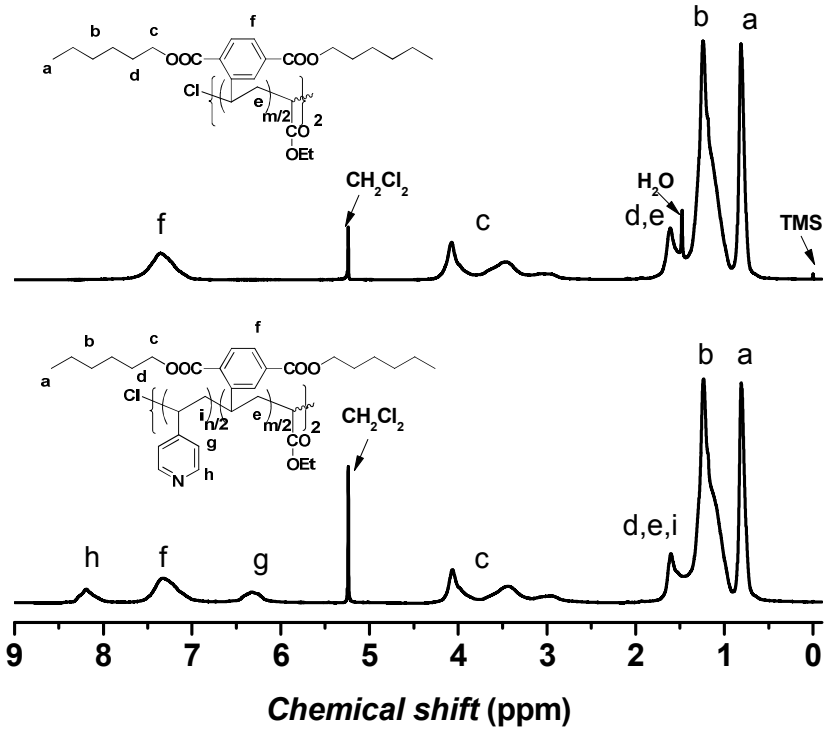

Fig. 1 Typical ^{1}H NMR spectra (400 MHz) of Cl-PHCS-Cl (degree of polymerization of 123, upper panel) and P4VP-*b*-PHCS-*b*-P4VP (sample $V_{30}H_{123}V_{30}$, lower panel) in CD_2Cl_2.

After optimizing the polymerization condition, the triblock copolymers of P4VP-*b*-PHCS-*b*-P4VP with different MW and compositions were successfully obtained. All the GPC traces of the resultant triblocks were unimodal, with the retention times obviously shorter compared with that of macroinitiator (see Fig. SI-3 in Supporting Information). It should be noted that when pure THF was used as the eluent, P4VP block can adsorb to the column material of GPC. This adsorption can cause the broadening of GPC traces and also the baseline shifting, leading to the apparently larger PDI which is of around 1.4. Fig. 1 shows a typical ^{1}H NMR spectrum (lower panel) of a triblock sample obtained, also suggesting the success of the triblock synthesized. Using the resonances of -OCH_2 protons (δ = 3.0-4.0 ppm) in the PHCS block and that of protons on the pyridine ring (δ = 8.0-9.0 ppm, or 6.0-7.0 ppm), we can estimate the composition of PHCS and P4VP based on the ^{1}H NMR result. The weight fraction of the P4VP block (w_{P4VP}) was calculated according to Eq. 1:

$$w_{P4VP} = 2I_h \times M_{4VP} / [2I_h \times M_{4VP} + I_c \times M_{HCS}] \quad (1)$$

where M_{4VP} of 105 g mol^{-1} and M_{HCS} of 360 g mol^{-1} are the molar masses of the two repeating units, I_h and I_c are the integral intensities of the signals at 8.0 to 9.0 and 3.0 to 4.0 ppm shown in Fig. 1. The MW of P4VP can be calculated based on the MW of PHCS measured by LS-GPC and w_{P4VP} by ^{1}H NMR. Furthermore, we estimated the volume fraction of P4VP (f_{P4VP}) using Eq. 2:

$$f_{P4VP} = 1.04 \times w_{P4VP} / [(1.04 - 1.17) \times w_{P4VP} + 1.17] \quad (2)$$

where 1.04 g cm^{-3} and 1.17 g cm^{-3} are the densities of PHCS and P4VP, respectively. The molecular characterization results of the P4VP-*b*-PHCS-*b*-P4VP samples studied in this paper are listed in Table 1. The sample code shown Table 1 and below reads "$V_XH_YV_X$", wherein the subscripts of X and Y are the degrees of polymerization (DPs) of PHCS and P4VP block, respectively. To obtain the triblock with the typical elastomeric property, the f_{P4VP} was controlled lower than 20%. While the f_{P4VP} exceeded 20% the sample became more or less brittle (for example, $V_{60}H_{84}V_{60}$ (f_{P4VP} = 26.7%) gave the ultimate tensile strength of 5.1 MPa and tensile strain at break of 60%).

Table 1. Molecular characterization data P4VP-*b*-PHCS-*b*-P4VP

Sample code [a]	Conversion	$M_{n,GPC}$ [b] (kg mol^{-1})	PDI [b]	$M_{n,NMR}$ [c] (kg mol^{-1})	w_{P4VP} [d]	f_{P4VP} [e]
$V_{17}H_{51}V_{17}$	40%	26.0	1.41	21.9	15.9	14.4
$V_{22}H_{77}V_{22}$	35%	32.1	1.39	32.3	14.5	13.1
$V_{36}H_{77}V_{36}$	48%	32.6	1.33	35.1	21.4	19.5
$V_{30}H_{123}V_{30}$	45%	43.2	1.39	50.9	12.5	11.3
$V_{26}H_{130}V_{26}$	38%	46.7	1.37	52.4	10.5	9.4
$V_{55}H_{157}V_{55}$	35%	50.6	1.37	68.2	17.0	15.5

[a] Sample code $V_XH_YV_X$, where the subscripts X and Y are the DPs for P4VP and PHCS, respectively. [b] Apparent MW of triblocks by GPC calibrated with PS standard, THF as eluent. [c] MW of triblocks measured by LS-GPC and ^{1}H NMR. [d] Calculated according to Eq. 1. [e] Calculated according to Eq. 2.

Phase morphologies of P4VP-*b*-PHCS-*b*-P4VP. In order to obtain the ABA triblock copolymer with the properties of TPE, microphase separated structure should be constructed by designing the two components appropriately. The A and B block employed have to be immiscible, guaranteeing that the triblock can undergo microphase separation to form the soft rubbery phase and the hard thermoplastic microdomains which can act as "physical cross-links" for the rubbery matrix. In our system, PHCS was selected to be the inner soft block as its unique LC phase behavior might bring some new features to the TPE. The usually used hard segment of PS was also employed in our experiments at first, as it could be synthesized more easily. However, the copolymer containing PS and PHCS block could only segregate weakly, particularly when the PS content was controlled to be minor. We expected that P4VP with the polar pendant group of pyridine and PHCS should exhibit stronger separation tendency. The homopolymers of PHCS and P4VP underwent macrophase separation when they were blended together, indicating that P4VP is immiscible with PHCS. P4VP possesses the T_g of ~140°C, nearly 40 °C higher than that of PS. Moreover, its pyridine sites can complex with other species such as metal salts or carboxylic acid via non-covalent interaction, and thus the properties of P4VP domains in a copolymer can be readily tuned. Therefore, using P4VP to replace the conventional hard segment of PS in the ABA type TPE is attractive.

Table 2. Glass transition and phase morphology of P4VP-*b*-PHCS-*b*-P4VP

Sample code	$T_{g1,\ PHCS}$ [a] (°C)	$T_{g2,\ P4VP}$ [a] (°C)	q_1(nm^{-1}) [b]	D (nm) [c]	Morphology [d]
$V_{17}H_{51}V_{17}$	-9.1	108.8	0.45	14.0	spherical
$V_{22}H_{77}V_{22}$	-18.9	116.3	0.31	20.1	spherical
$V_{36}H_{77}V_{36}$	-16.0	138.3	0.27	23.3	cylindrical
$V_{30}H_{123}V_{30}$	-11.0	126.7	0.26	24.2	cylindrical
$V_{26}H_{130}V_{26}$	-14.9	126.9	0.25	25.1	spherical

$V_{55}H_{157}V_{55}$	-15.2	127.0	0.21	29.9	-

[a] Determined from tanδ of the DMA result. [b] Position of first-order scattering observed by SAXS at room temperature. [c] *d*-spacing corresponding to q_1. [d] Phase morphology determined based on the combination of SAXS and TEM results.

Thermal behaviors of P4VP-*b*-PHCS-*b*-P4VP were first examined by DSC. The T_g of PHCS in the triblocks was found at around -25 °C, slightly higher than that around -30 °C of the homo-PHCS. For the triblock with the P4VP content higher than 25%, a glass transition at around 130 °C could be clearly observed, which is attributed to the P4VP block (Fig. SI-5 in Supporting Information). However, with the P4VP content lower than 20%, the triblocks could not render clearly glass transition process of P4VP on the DSC traces recorded upon either cooling or heating. We further employed DMA to identify the glass transitions of the triblocks. Shown in Fig. 2a are the storage modulus (*G*'), loss modulus (*G*"), and tanδ of $V_{36}H_{77}V_{36}$ (f_{P4VP} = 19.5%) as functions of temperature. In the temperature range investigated, *G*' displays two steps of decrease during the heating process at a rate of 3 °C min^{-1}. According to the curve of tanδ, the temperatures of two peaks can be assigned to the T_gs of PHCS and P4VP block, which are at -16 and 138 °C, respectively. The two distinct glass transitions corresponding to the PHCS and P4VP indicate microphase separation of the triblock. The T_g of PHCS obtained by DMA is higher than that measured by DSC. In DMA measurement, the sample was subjected to cyclic loading, and thus the chains became flexible at relatively higher temperatures compared to that in DSC.[51] From Fig. 2b, we observe that increase of the MW of P4VP can cause the increment of T_g of P4VP. On the other hand, with a similar f_{P4VP}, the triblocks exhibit almost identical T_g of PHCS when the M_n of PHCS is higher than 25k g mol^{-1} (Table 2).

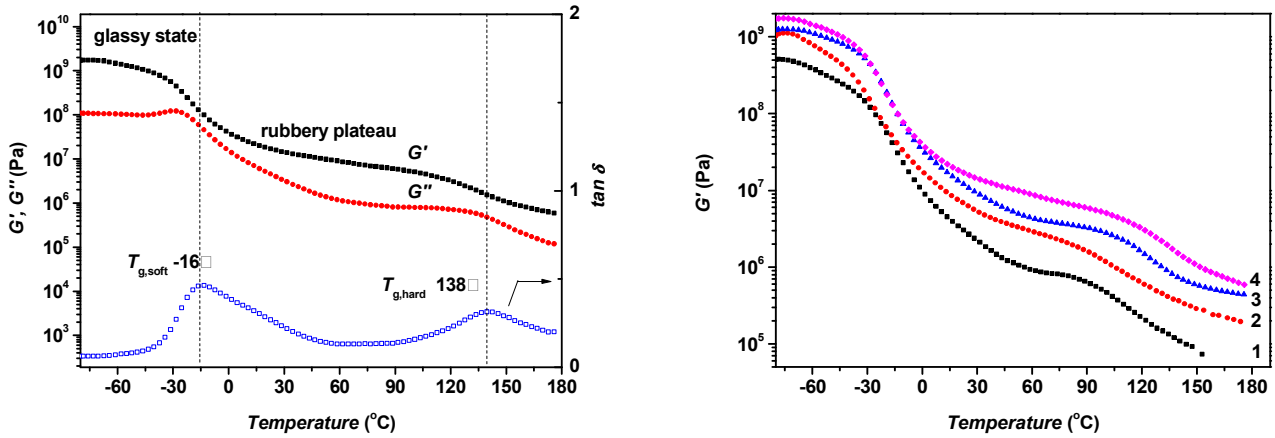

(a) **(b)**

Fig. 2 (a) DMA result of the triblock $V_{36}H_{77}V_{36}$. (b) Comparison of the thermomechanical properties of different triblock samples. (1) $V_{17}H_{51}V_{17}$ (f_{P4VP} = 14.4%), (2) $V_{22}H_{77}V_{22}$ (f_{P4VP} = 13.1%), (3) $V_{30}H_{123}V_{30}$ (f_{P4VP} = 11.3%), (4) $V_{36}H_{77}V_{36}$ (f_{P4VP} = 19.5%). For (1), (2), and (3), the samples possess similar content of P4VP but different total MW; for (2) and (4), the samples possess similar PHCS block but different content of P4VP.

The DSC and DMA results suggest the existence of microphase separation of P4VP-*b*-PHCS-*b*-P4VP. To further investigate the phase morphologies, we carried out SAXS experiments. The samples were annealed in vacuum for 24 h at 160 °C, where is above the T_g of P4VP blocks but far below the decomposition temperature of 320 °C. Typical SAXS profiles of the samples are shown in Fig. 3, evidencing the microphase separation of the triblocks we synthesized. Increasing the total MW of the triblock results in the peak position of the first-order scattering (q_1) shifting to lower angles, indicating that the periodicity of microphase separated structure becomes larger. Varying the composition of triblock can change the phase morphology. For instance, the samples of $V_{30}H_{123}V_{30}$ and $V_{26}H_{130}V_{26}$ possess the inner PHCS block with a similar MW. While the former one (f_{P4VP} = 11.3%) exhibits two scattering peaks with the q-ratio of 1:√3, three scattering peaks can be fairly observed for the later one with f_{P4VP} of 9.4%, which follows the q-ratio of 1:√2:√3. Therefore, the two samples should form the cylindrical and spherical morphology, respectively. We also note that some of the triblock samples just present the higher-order scatterings weak and diffusive, implying that the long-range order was just

poorly developed. This may be mainly due to that the samples possess a relatively large MW distribution.[52] Also, existence of the residue homo-PHCS which was the macroinitiator and some diblocks of PHCS-b-P4VP formed during the ATRP chain extension reaction may cause the microphase separation imperfect.

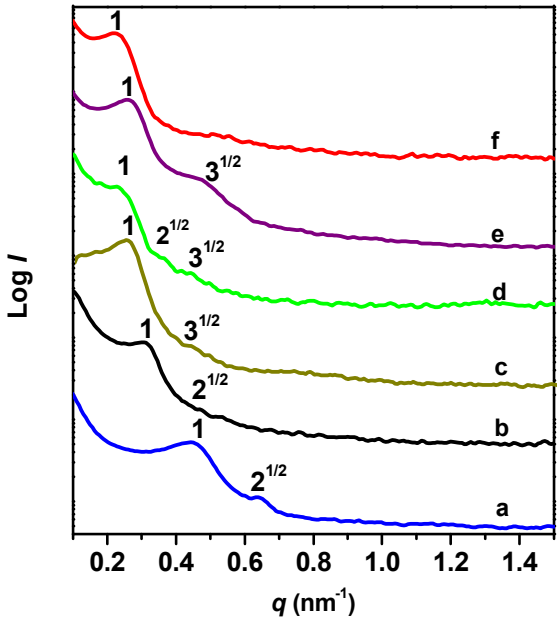

Fig. 3 SAXS profiles of P4VP-b-PHCS-b-P4VP samples. (a) $V_{17}H_{51}V_{17}$ (f_{P4VP} = 14.4%), (b) $V_{22}H_{77}V_{22}$ (f_{P4VP} = 13.1%), (c) $V_{36}H_{77}V_{36}$ (f_{P4VP} = 19.5%), (d) $V_{26}H_{130}V_{26}$ (f_{P4VP} = 9.4%), (e) $V_{30}H_{123}V_{30}$ (f_{P4VP} = 11.3%), (f) $V_{55}H_{157}V_{55}$ (f_{P4VP} = 15.5%).

We intended to identify the phase structures of triblocks by combining the SAXS and TEM results. The TEM samples were prepared by microtome followed by staining with RuO_4. Since it was easier to be stained, the P4VP domain looked darker under TEM compared to the PHCS domain. The TEM images corresponding to the samples used in Fig. 3 are presented in Fig. 4. For $V_{17}H_{51}V_{17}$ (f_{P4VP} = 14.4%) with the two distinct scatterings at 0.45 and 0.64 nm^{-1} (i.e., the q-ratio of 1:$\sqrt{2}$), Fig. 4a shows that the P4VP spheres are dispersed in the PHCS matrix. Similar morphology is observed for $V_{22}H_{77}V_{22}$ (f_{P4VP} = 13.1%) (Fig. 4b) and $V_{26}H_{130}V_{26}$ (f_{P4VP} = 9.4%) (Fig. 4d), suggesting that these two also form the sphere phase. However, the TEM images revealed the lack of long-range ordering of the microphase

separation structure. The dark domain looks larger, which should be due to that the PHCS blocks were also stained to some extent. For $V_{36}H_{77}V_{36}$ (f_{P4VP} = 19.5%) and $V_{30}H_{123}V_{30}$ (f_{P4VP} = 11.3%), both the dark dots and dark lines can be seen in Fig. 4c and 4e, respectively. Moreover, the dark dots are arranged in the matrix with the hexagonal symmetry. These observations indicate the cylinder phase (also see Fig. SI-6 in Supporting Information), consistent with the SAXS results showing the scatterings with the q-ratio of 1: √ 3.

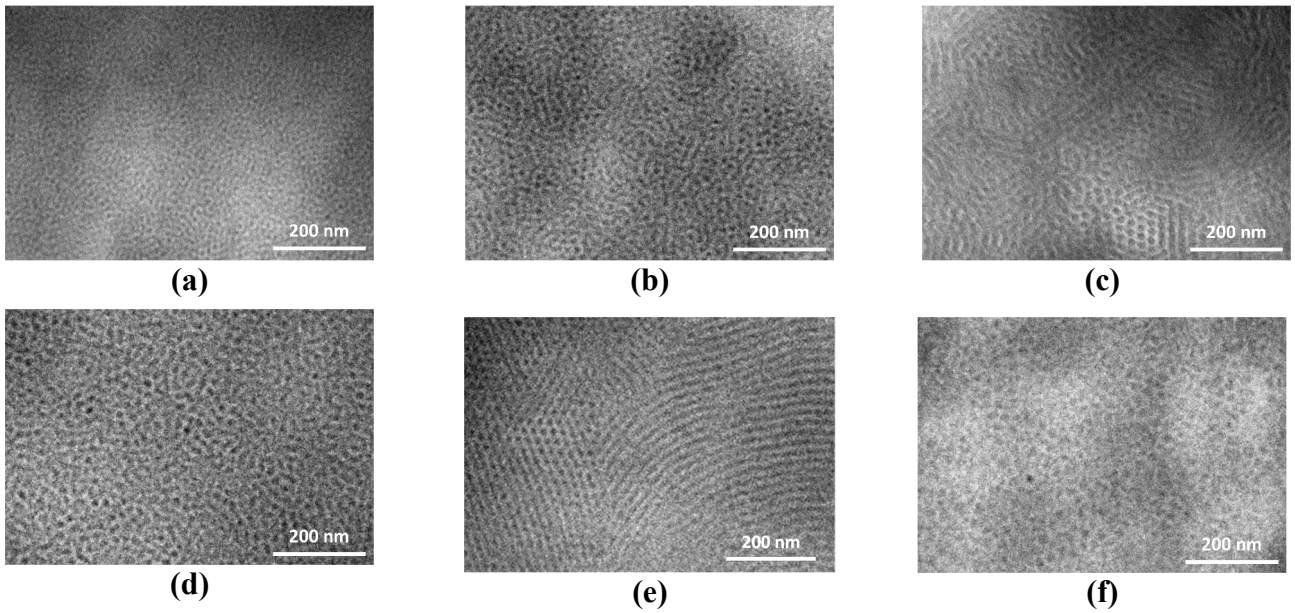

Fig. 4 TEM image of P4VP-b-PHCS-b-P4VP samples. (a) $V_{17}H_{51}V_{17}$ (f_{P4VP} = 14.4%), (b) $V_{22}H_{77}V_{22}$ (f_{P4VP} = 13.1%), (c) $V_{36}H_{77}V_{36}$ (f_{P4VP} = 19.5%), (d) $V_{26}H_{130}V_{26}$ (f_{P4VP} = 9.4%), (e) $V_{30}H_{123}V_{30}$ (f_{P4VP} = 11.3%), (f) $V_{55}H_{157}V_{55}$ (f_{P4VP} = 15.5%). To enhance contrast between the soft and hard phase, the samples were stained with RuO_4 vapor.

The phase identifications of the triblocks are summarized in Table 2. It is noted that for the samples with relatively low total MW (e.g., $V_{22}H_{77}V_{22}$), reducing the f_{P4VP} to below 15% can result in the spherical phase; however, the sample of $V_{30}H_{123}V_{30}$ (f_{P4VP} = 11.3%) which possesses a smaller f_{P4VP} of 11.3% remains the cylinder phase. This shall be because that the larger total MW gives the larger value of χN (χ is the Flory-Huggins interaction parameter and N the degree of polymerization of triblock), leading to a wider composition range of cylinder phase. For the sample with the highest MW, namely,

$V_{30}H_{123}V_{30}$, the primary scattering peak observed corresponds to a *d*-spacing of 29.9 nm. However, the higher-order scatterings of the sample were hard to be detected, and no TEM image with typical morphology was obtained (Fig. 4f). Therefore, its phase morphology remains unclear.

From the X-ray scattering profiles, we could find that all the samples give a scattering halo at q = 3.60 nm^{-1}, which is attributed to the PHCS block (Fig. SI-7 in Supporting Information). The homo-PHCS with sufficiently high MW exhibits an interesting LC behavior with the feature of "isotropic re-entry". Namely, its LC phase of Φ_H can develop upon heating to above ~100 °C, evidenced by the a sharp diffraction peak appearing at the q of 3.79 nm^{-1};[35] during cooling to room temperature or below, the LC diffraction peak will disappear, resulting in an amorphous state. For all the triblocks synthesized, we found that the PHCS blocks always gave the scattering halo, even when the samples were heated to 200 °C, indicating no LC ordering of PHCS developed. This may be mainly due to that the MW of PHCS block is not high enough (e.g., higher than 100 kg mol^{-1}), and thus the cylindrical conformation of PHCS chains cannot be stabilized.[35] On the other hand, the microphase separated structures of the triblock might also disfavor the LC phase formation of PHCS in the quiescent condition.

Mechanical properties of P4VP-*b*-PHCS-*b*-P4VP. Microphase separation caused by the incompatibility between P4VP and PHCS block enhances mechanical properties. The homo-PHCS with a T_g of -30 °C is sticky and easy to flow at room temperature, while the homo-P4VP is quite brittle. P4VP-*b*-PHCS-*b*-P4VP with f_{P4VP} lower than 20% can show the feature of elastomer. Its elastic behavior is largely affected by the total MW of the triblock and the composition of P4VP.

As shown in Fig. 2b of the DMA results, the triblocks are typical glassy at below the T_g of PHCS, with G' of ~1 GPa. Above this T_g, the copolymers become elastic and show a rubbery plateau with a G' of ~10 MPa extending up to the softening temperature of P4VP. The existence of the rubbery plateau shall be attributed to that the P4VP blocks form glassy domains that connect the soft PHCS segments.

The height of the plateau strongly depended on the P4VP content. When the length of inner soft segment is fixed, the sample with a lower P4VP content has a smaller *G*' in the rubbery plateau region. In Fig. 2b, curve 2 and curve 4 show that at room temperature the *G*' values of $V_{22}H_{77}V_{22}$ (f_{P4VP} = 13.1%) and $V_{36}H_{77}V_{36}$ (f_{P4VP} = 19.5%) are 6.6 and 18.7 MPa, respectively. It is also noted that the latter one has the T_g of P4VP significantly higher than the former one (138.3 °C vs. 116.3 °C), and thus has a wider plateau region. These observations confirm that the elasticity and the thermal property of the triblock can be tuned by controlling the content of hard segment when the inner soft PHCS is fixed. In Fig. 2b, curves 1, 2, and 3 of *G*' vs. temperature correspond to three triblocks of $V_{17}H_{51}V_{17}$ (f_{P4VP} = 14.4%), $V_{22}H_{77}V_{22}$ (f_{P4VP} = 13.1%), and $V_{30}H_{123}V_{30}$ (f_{P4VP} = 11.3%), respectively, which have similar P4VP contents (10% < f_{P4VP} < 15%) but different total MW. With increasing the total MW, the *G*' values at room temperature increase from 2.8 to 6.3 and to 10.9 MPa. Moreover, the sample with the lowest total MW (i.e., $V_{17}H_{51}V_{17}$) possesses the lowest *G*' in the whole temperature range in comparison with the others.

The increase of total MW also has a positive impact on the tensile property. Fig. 5a depicts the stress-strain curves of three triblocks with the f_{P4VP} of around 14%. It can be seen that both the ultimate tensile strength and the elongation at break of the triblocks increase with increasing the total MW, which reach 6.6 MPa and 400% for the sample of $V_{55}H_{157}V_{55}$ (f_{P4VP} = 15.5%) (see Table 3). The samples show a ductile failure under elongation with a moderate tensile strength, a common feature of TPE. Assuming that the PHCS block might develop into LC phase when the triblock was subjected to elongation, we attempted to see if the LC formation can offer some unique mechanical properties to the P4VP-*b*-PHCS-*b*-P4VP. However, even for the sample with the highest MW of PHCS synthesized, i.e., $V_{55}H_{157}V_{55}$, we just observed a normal behavior of TPE.

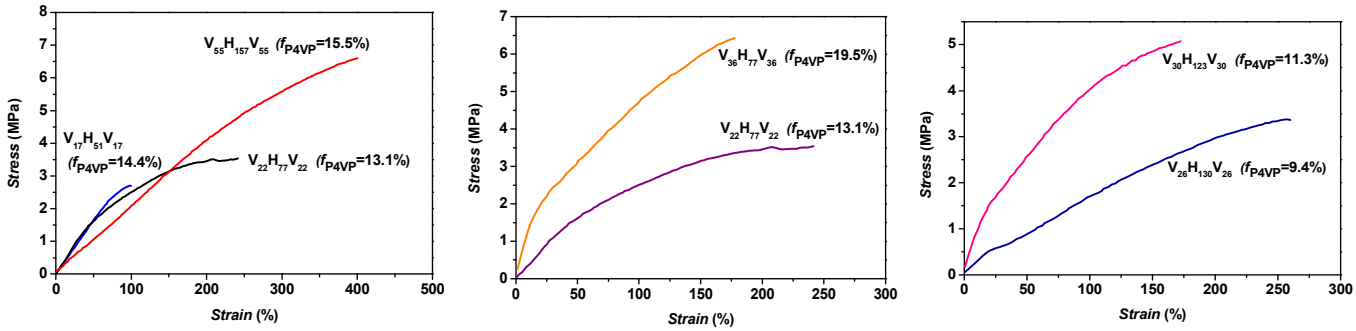

(a) **(b)** **(c)**

Fig. 5 Stress-strain curves of P4VP-*b*-PHCS-*b*-P4VP. (a) The sample with similar compositions but significantly different MWs. (b) and (c), The sample with similar MW of the soft segments but different hard phase compositions.

It is known that the composition also has a major effect on the tensile properties of the ABA triblock copolymers. As shown in Fig. 5b of $V_{22}H_{77}V_{22}$ (f_{P4VP} = 13.1%) and $V_{36}H_{77}V_{36}$ (f_{P4VP} = 19.5%), with the MW of inner soft segment fixed, increasing the P4VP content resulted in a significant increase of ultimate tensile strength but a sacrifice of elongation at break. Same situation can be found from the comparison between $V_{26}H_{130}V_{26}$ (f_{P4VP} = 9.4%) and $V_{30}H_{123}V_{30}$ (f_{P4VP} = 11.3%) (Fig. 5c). The limitations in the tensile properties of triblock copolymers may be related to the intrinsic brittleness of the P4VP hard segment. It should be noted that $V_{22}H_{77}V_{22}$ (f_{P4VP} = 13.1%) and $V_{26}H_{130}V_{26}$ (f_{P4VP} = 9.4%) form a sphere phase, while $V_{36}H_{77}V_{36}$ (f_{P4VP} = 19.5%) and $V_{30}H_{123}V_{30}$ (f_{P4VP} = 11.3%) form a cylinder phase. While in Fig. 2b no obvious dependence of the *G*' on the phase morphology can be seen, we can see from Fig. 5 that the triblocks with a sphere phase can elongate more than that with a cylinder phase. For the triblocks sharing same phase morphology, the higher the MW of P4VP, the higher ultimate tensile strength will be. The tensile properties of the samples are summarized in Table 3.

Table 3. Tensile properties of P4VP-*b*-PHCS-*b*-P4VP

Sample code	Ultimate tensile strength (MPa)	Tensile strain at break (%)
$V_{17}H_{51}V_{17}$	2.70	99.7

$V_{22}H_{77}V_{22}$	3.05	241.7
$V_{36}H_{77}V_{36}$	6.43	177.5
$V_{26}H_{130}V_{26}$	5.07	172.6
$V_{30}H_{123}V_{30}$	3.36	260.0
$V_{55}H_{157}V_{55}$	6.60	400.5

P4VP-*b*-PHCS-*b*-P4VP/Zn(ClO$_4$)$_2$ complex. To tune the thermal and mechanical properties of P4VP-*b*-PHCS-*b*-P4VP, one can take advantage of the P4VP block which can complex with other organic and inorganic species via non-covalent bonding interaction.[44,45,53-57] It has been reported by Kuo et al. that P4VP can well complex with $Zn(ClO_4)_2$, resulting in a hybrid with enhanced thermal and mechanical properties.[58] Using the triblock of $V_{30}H_{123}V_{30}$, we prepared the P4VP-*b*-PHCS-*b*-P4VP/$Zn(ClO_4)_2$ complex samples (Scheme 3) by solution blending. For pure $V_{30}H_{123}V_{30}$, the cylinder phase morphology has been well evidenced by SAXS and TEM experiments. This allows us to elucidate more clearly how the phase morphology will change with adding different amount of salt. The blending samples are denoted as $Zn^{2+}/V_{30}H_{123}V_{30}$ (x:y), where x:y is the molar ratio of Zn^{2+} to the repeating unit of P4VP. The coordination interaction between pyridine and Zn^{2+} can be confirmed by FTIR.[54,58] Two distinct absorption peaks for the pyridine ring stretching mode of pure P4VP exist at 1590 and 992 cm^{-1}, respectively. Upon addition of $Zn(ClO_4)_2$, new bands appear at 1616 cm^{-1} and 1033 cm^{-1} (Fig. SI-8 in Supporting Information), which should be due to the zinc cation coordinating with pyridine rings.

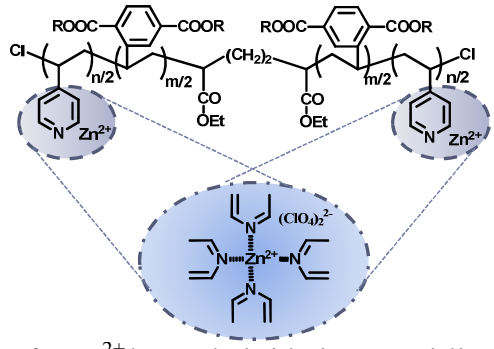

Scheme 3 Schematic illustration of a Zn^{2+}/VHV hybrid via mental-ligand complexation.

Adding $Zn(ClO_4)_2$ into $V_{30}H_{123}V_{30}$ can indeed change the phase morphology substantially. The cylinder phase of $V_{30}H_{123}V_{30}$ renders the first-order scattering located at q_1 = 0.26 nm^{-1} (*d*-spacing of 24.2 nm). As shown in Fig. 6 of the SAXS results, after complexation with $Zn(ClO_4)_2$, the samples give the first-order scattering continuously shifting to lower *q* side with increasing the amount of salt. At a molar ratio of 1:6, the first-order scattering is peaked at q = 0.19 nm^{-1}. For $Zn^{2+}/V_{30}H_{123}V_{30}$ (1:18), two scatterings with the *q*-ratio of 1:√3 can be identified. However, adding more the salt will eventually lead to the *q*-ratio of the scatterings changing to 1:2, indicating a lamellar phase.

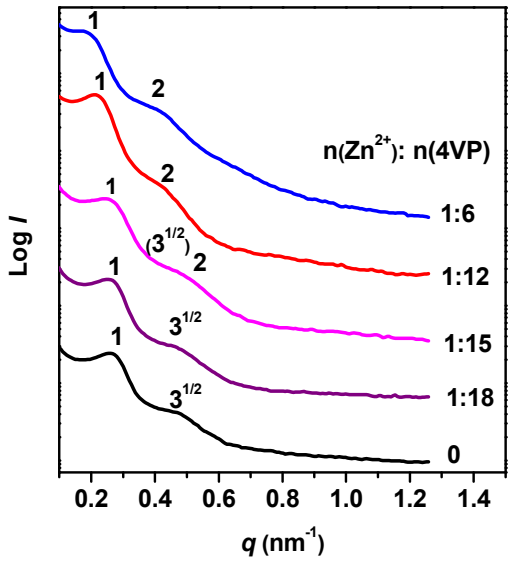

Fig. 6 SAXS profiles of pure $V_{30}H_{123}V_{30}$ and the hybrids of $Zn^{2+}/V_{30}H_{123}V_{30}$ (x:y). From bottom to top, the ratios of x:y are of 0, 1:18, 1:15, 1:12, 1:6.

Fig. 7 shows the TEM pictures of $Zn^{2+}/V_{30}H_{123}V_{30}$ (x:y). While dark dots and short cylinders can be observed in $Zn^{2+}/V_{30}H_{123}V_{30}$ (1:18) (Fig. 7a), the sample of $Zn^{2+}/V_{30}H_{123}V_{30}$ (1:15) seems to present both cylinders and lamellae (Fig. 7b), indicating a not well developed lamellar phase, or the coexistence of cylinder phase and lamellar phase. For $Zn^{2+}/V_{30}H_{123}V_{30}$ (1:12), the TEM picture (Fig. 7c) shows that the dark lines parallel to each other are not very long and the ordered domains look not large, implying the lamellar phase is still more or less disordered. When the amount of metal salt is further increased,

$Zn^{2+}/V_{30}H_{123}V_{30}$ (1:6) exhibit the typical morphology of lamellar phase (Fig. 7d). The phase morphology changing from cylinder to lamella shall be attributed to the incorporation of zinc salt. As $Zn(ClO_4)_2$ complexed with the nitrogen in pyridine ring, the ions strongly affect the conformation of P4VP chains and lead to the significant increase in excluded volume rather than the simple swelling by the intrinsic volume of the zinc salt. The strong association of the metal-ligand complex profoundly creates extra volume in the P4VP microdomains so as to cause the phase morphology transformation and domain spacing expansion.[41,59]

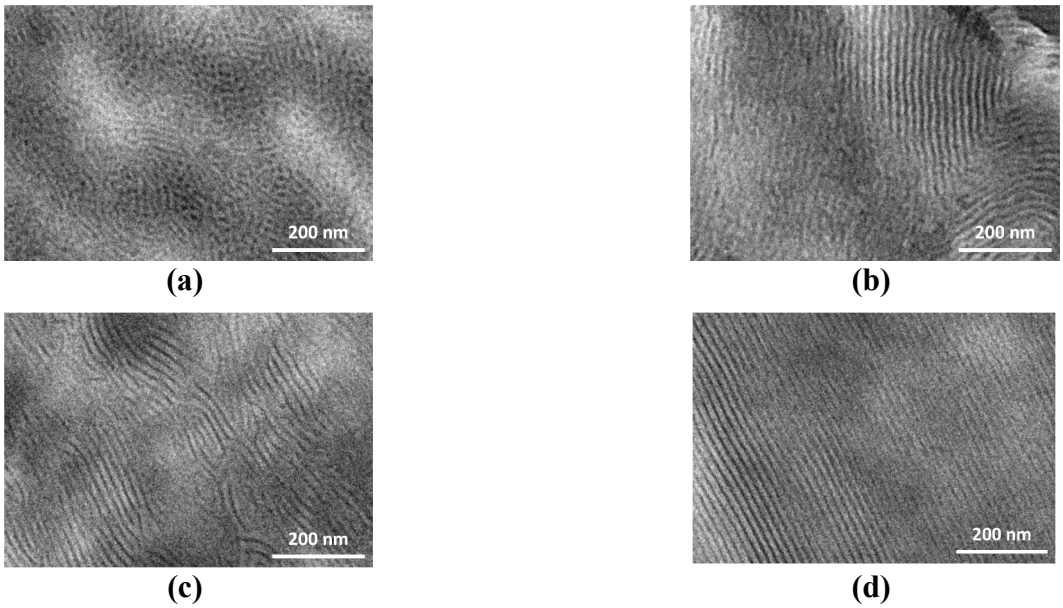

Fig. 7 TEM images of $Zn^{2+}/V_{30}H_{123}V_{30}$ (x:y). The ratios of x:y are (a) 1:18, (b) 1:15, (c) 1:12, and (d) 1:6. To enhance contrast between the soft and hard phase, the samples were stained with RuO_4 vapor.

The metal-ligand complexation of P4VP and $Zn(ClO_4)_2$ influenced the thermal and mechanical properties greatly. Fig. 8 shows the tensile property of the $Zn^{2+}/V_{30}H_{123}V_{30}$ (x:y) samples. The ultimate tensile strengths of all the complexed samples prepared are around 5 MPa, similar to that of the pure $V_{30}H_{123}V_{30}$. As the amount of zinc salt increased, the elongation at break decreased dramatically. For $Zn^{2+}/V_{30}H_{123}V_{30}$ (1:12) and $Zn^{2+}/V_{30}H_{123}V_{30}$ (1:6), which can form lamellar phases, it is obvious that the modulus is much larger than that of pure triblock. Fig. 9 describes the DMA results of $Zn^{2+}/V_{30}H_{123}V_{30}$

(x: y). As Zn^{2+} in fact can act as a cross-linking agent within the P4VP domain, the hard phase of the triblock is enhanced, resulting in the raising of *G*' of the rubbery plateau. At 50 °C, the value of *G*' increases from 5.3 MPa for the pure $V_{30}H_{123}V_{30}$ to 13.0 MPa for $Zn^{2+}/V_{30}H_{123}V_{30}$ (1:6). The most important enhancement is the extended rubbery plateau. For the pure triblock, the end of the rubbery plateau, where the *G*' starts to decrease, is about 100 °C. However, for the blend samples with x:y of 1:18, 1:12, and 1:6, the decrease of *G*' takes place at 130, 150, and 220 °C, respectively, indicating a greatly enhanced thermal stability.

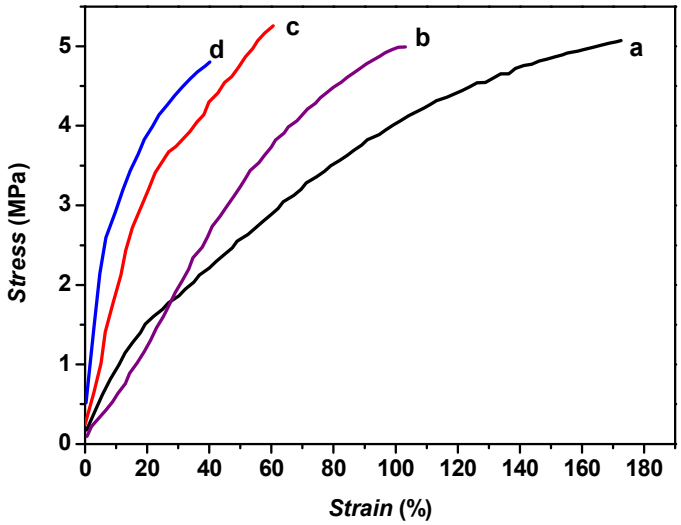

Fig. 8 Stress-strain curves of $Zn^{2+}/V_{30}H_{123}V_{30}$ (x:y). The ratios of x:y are (a) 0, (b) 1:18, (c) 1:12, and (d) 1:6.

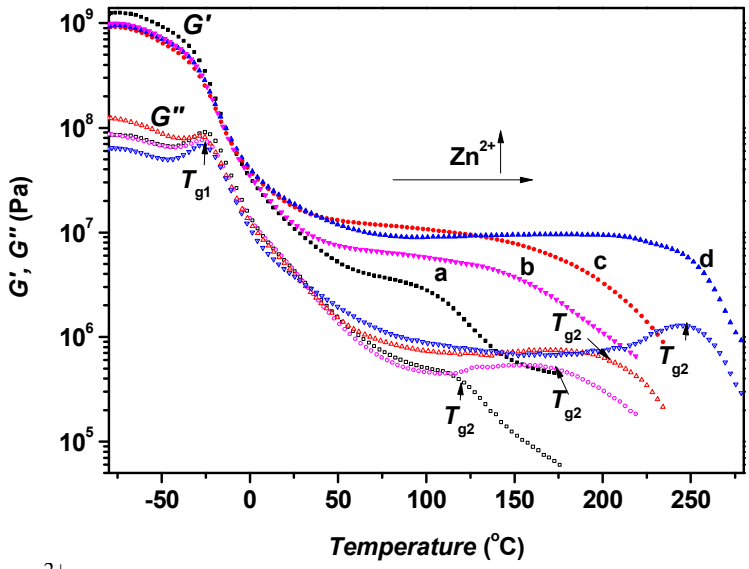

Fig. 9 DMA results of Zn^{2+}/VHV (x:y). The ratios of x:y are (a) 0, (b) 1:18, (c) 1:12, and (d) 1:6.(solid dot: storage modulus *G*', open dot: loss modulus *G*"). T_{g1} and T_{g2} are T_gs of PHCS block and hard phase, respectively.

As shown in Fig. 9, the T_g of PHCS, which corresponds to the first drop of *G*', is little affected by adding the zinc salt. Therefore, the widening of the rubbery plateau of $Zn^{2+}/V_{30}H_{123}V_{30}$ (x:y) is mainly caused by the substantially increased T_g of the hard phase. The mobility of P4VP block becomes restricted after complexed with Zn^{2+}. According to *G*" shown in Fig. 9, the T_g of hard phase of $Zn^{2+}/V_{30}H_{123}V_{30}$ (1:18) is found to be 168 °C, 52 °C higher than that of pure $V_{30}H_{123}V_{30}$. For x:y = 1:6, the T_g of hard phase even reaches 247 °C. However, with such a high T_g, $Zn^{2+}/V_{30}H_{123}V_{30}$ (1:6) becomes brittle and its elongation at break is of ~40%. Therefore, to obtain the overall good performance of the triblock we synthesized, the amount of zinc salt added should be carefully chosen. For example, according to the data shown in Fig. 8 and Fig. 9, $Zn^{2+}/V_{30}H_{123}V_{30}$ (1:18) exhibits the thermal stability better than the pure $V_{30}H_{123}V_{30}$. On the other hand, when the cylinder phase is remained, the sample has the tensile properties decreased not too much, compared with those containing more zinc salt with the phase morphology changed to lamellae. In general, blending salt with the P4VP-*b*-PHCS-*b*-P4VP can be

considered as a facial way to strengthen the hard phase of P4VP, which can give a much better thermal stability of the materials.

Conclusion

In summary, linear ABA triblock copolymers containing inner soft PHCS block and outer hard P4VP block with different MWs and compositions have been synthesized by ATRP with the aid of halogen exchange. Microphase separated morphology of cylindrical or spherical P4VP domains arranged in the PHCS matrix are observed when f_{P4VP} is less than 20%, and the triblock can be used as a stable thermoplastic elastomer. Balancing the parameters such as MW and volume fraction of P4VP can tune the morphology and thermomechanical properties of P4VP-*b*-PHCS-*b*-P4VP. Incorporation of $Zn(ClO_4)_2$ to the triblock copolymer induces a significant change of phase morphology as well as expansion of domain spacing. The hybrids of triblock and zinc salt show greatly improved thermal stability, the modules much higher than the pure triblock copolymer, along with a sacrifice of elongation at break. To find a balance, the complex with only a little amount of metal salt should be a good candidate, as it has both good elastic property and thermal stability. In the present work, probably due to the MW of inner segment is not high enough, the LC properties of PHCS with an "isotropic re-entry" feature did not observed. Nevertheless, it is still intriguing to explore how the orientation of inner soft phase and LC phase formation impact on the phase morphology and mechanical properties of the PHCS containing triblock copolymers. The research on this line is ongoing in our laboratory.

Acknowledgements

This work was supported by the National "973" Project (No. 2011CB606004) and National Natural Science Foundation of China (No. 20990232)

Notes and references

(1) F. S. Bates and G. H. Fredrickson, Phys. Today., 1999, **52**, 32.

(2) G. M. Whitesides and B. Grzybowski, Science, 2002, **295**, 2418-2421.

(3) A. Noro, Y. Nagata, M. Tsukamoto, Y. Hayakawa, A. Takano and Y. Matsushita, Biomacromolecules, 2005, **6**, 2328-2333.

(4) J. Bang, U. Jeong, D. Y. Ryu, T. P. Russell and C. Hawker, J. Adv. Mater. 2009, **21**, 4769-4792.

(5) S. B. Darling, Prog. Polym. Sci. 2007, **32**, 1152-1204.

(6) J. M. Widin, A. K. Schmitt, A. L. Schmitt, K. Im and M. K. Mahanthappa, J. Am. Chem. Soc. 2012, **134**, 3834-3844.

(7) R. J. Spontak and N. P. Patel, Curr. Opin. Colloid. In. 2000, **5**, 333-340.

(8) M. W. Matsen and R. B. Thompson, J. chem. phys. 1999, **111**, 7139.

(9) M. W. Matsen, J. Chem. Phys. 2000, **113**, 5539.

(10) N. Sota, N. Sakamoto, K. Saijo and T. Hashimoto, Macromolecules 2003, **36**, 4534-4543.

(11) L. J. Fetters and M. Morton, Macromolecules 1969, **2**, 453-458.

(12) H. Schmalz, V. Abetz and R. Lange, Compos. Sci. Technol. 2003, **63**, 1179-1186.

(13) B. J. Dair, C. C. Honeker, D. B. Alward, A. Avgeropoulos, N. Hadjichristidis, L. J. Fetters, M. Capel and E. L. Thomas, Macromolecules 1999, **32**, 8145-8152.

(14) Y. Orimo and A. Hotta, Macromolecules 2011, **44**, 5310-5317.

(15) C. W. Bielawski and R. H. Grubbs, Prog. Polym. Sci. 2007, **32**, 1-29.

(16) T. Lebarbe, E. Ibarboure, B. Gadenne, C. Alfos and H. Cramail, Poly. Chem. 2013. **4**, 3357-3369.

(17) S. Cheng, F. L. Beyer, B. D. Mather, R. B. Moore and T. E. Long, Macromolecules 2011, **44**, 6509–6517.

(18) Y. Luo, X. Wang, Y. Zhu, B. Li and S. Zhu, Macromolecules 2010, **43**, 7472-7481.

(19) A. Nese, J. Mosnáček, A. Juhari, J. A. Yoon, K. Koynov, T. Kowalewski and K. Matyjaszewski, Macromolecules 2010, **43,** 1227-1235.

(20) C. Moineau, M. Minet, P. Teyssié and R. Jérôme, Macromolecules 1999, **32**, 8277-8282.

(21) B. Dufour, C. Tang, K. Koynov, Y. Zhang, T. Pakula and K. Matyjaszewski, Macromolecules 2008, **41**, 2451-2458.

(22) J. Mosnáček, J. Yoon, A. Juhari, K. Koynov and K. Matyjaszewski, Polymer 2009, **50**, 2087-2094.

(23) A. Juhari, J. Mosnáček, J. Yoon, A. Nese, K. Koynov, T. Kowalewski and K. Matyjaszewski, Polymer 2010, **51**, 4806-4813.

(24) S. Kobayashi, H. Kataoka, T. Ishizone, T. Kato, T. Ono, S. Kobukata and H. Ogi, Macromolecules 2008, **41**, 5502-5508.

(25) B. Dufour, K. Koynov, T. Pakula and K Matyjaszewski, Macromol. Chem. Phys. 2008, **209**, 1686-1693.

(26) J. M. Yu, P. Dubois and R. Jérôme, Macromolecules 1996, **29**, 8362-8370.

(27) J. Saenger and W. Gronski, Macromol. Chem. Phys. 1998, **199**, 555-561.

(28) S. Bai and Y Zhao, Macromolecules 2001, **34**, 9032-9038.

(29) S. Bai and Y Zhao, Macromolecules 2002, **35**, 9657-9664.

(30) L. Cui, X. Tong, X. Yan, G. Liu and Y. Zhao, Macromolecules 2004, **37**, 7097-7104.

(31) Y. Yi, X. Fan, X. Wan, L. Li, N. Zhao, X. Chen, J. Xu and Q. F. Zhou, Macromolecules 2004, **37**, 7610-7618.

(32) Q. F. Zhou, H. M. Li and X. D. Feng, Macromolecules 1987, **20**, 233-234.

(33) X. F. Chen, Z. Shen, X. H. Wan, X. H. Fan, E. Q. Chen, Y. Ma and Q. F. Zhou, Chem. Soc. Rev. 2010, **39**, 3072-3101.

(34) L. C. Gao, C. L. Zhang, X. Liu, X. H. Fan, Y. X. Wu, X. F. Chen, Z. Shen and Q. F. Zhou, Soft Matter 2008, **4**, 1230-1236.

(35) X. Yin, C. Ye, X. Ma, E. Chen, X. Qi, X. Duan, X. Wan, S. Z. Cheng and Q. Zhou, J. Am. Chem. Soc. 2003, **125**, 6854-6855.

(36) H. Tang, Z. Zhu, X. Wan, X. Chen and Q. Zhou, Macromolecules 2006, **39**, 6887-6897.

(37) Y. Zhao, X. Fan, X. Wan, X. Chen, Y. Yi, L. Wang, X. Dong and Q. Zhou, Macromolecules 2006, **39**, 948-956.

(38) C. Huang, S. Kuo, J. Chen and F. Chang, J. Polym. Res. 2005, **12**, 449-456.

(39) Q. Bo, X. Tong, Y. Zhao and Y. Zhao, Macromolecules 2008, **41**, 3562-3570.

(40) G. G. du Sart, R. Rachmawati, V. Voet, G. A. van Ekenstein, E. Polushkin, G. Ten Brinke and K. Loos, Macromolecules 2008, **41**, 6393-6399.

(41) T. Lin, R. M. Ho and J. C. Ho, Macromolecules 2009, **42**, 742-751.

(42) Y. Sageshima, S. Arai, A. Noro and Y. Matsushita, Langmuir 2012, **28**, 17524-17529.

(43) J. B. Beck, J. M. Ineman and S. J. Rowan, Macromolecules 2005, **38**, 5060-5068.

(44) L. A. Belfiore, M. P. McCurdie and E. Ueda, Macromolecules 1993, **26**, 6908-6917.

(45) A. Noro, Y. Sageshima, S. Arai and Y. Matsushita, Macromolecules 2010, **43**, 5358-5364.

(46) D. H. Lee, S. H. Han, W. Joo, J. K. Kim and J. Huh, Macromolecules 2008, **41**, 2577-2583.

(47) K. Matyjaszewski and J. Xia, Chem. Rev. 2001, **101**, 2921-2990.

(48) K. Matyjaszewski, Macromolecules 2012, **45**, 4015-4039.

(49) J. Xia, X. Zhang and K. Matyjaszewski, Macromolecules 1999, 32, 3531-3533

(50) J. Mosnáček and K. Matyjaszewski, Macromolecules 2008, **41**, 5509-5511.

(51) A. A. Kavitha and N. K. Singha, Macromolecules 2010, **43**, 3193-3205.

(52) J. M. Widin, A. K. Schmitt, K. Im, A. L. Schmitt and M. K. Mahanthappa, Macromolecules 2010,

43, 7913-7915.

(53) J. Ruokolainen, G. Ten Brinke, O. Ikkala, M. Torkkeli and R. Serimaa, Macromolecules 1996, **29**, 3409-3415.

(54) J. A. Orlicki, N. E. Zander and A. M. Rawlett, Army Research Lab Aberdeen Proving Ground Md Weapons and Materials Research Directorate 2010.

(55) T. Lin, C. Li, R. Ho and J. Ho, Macromolecules 2010, **43**, 3383-3391.

(56) A. Noro, K. Higuchi, Y. Sageshima and Y. Matsushita, Macromolecules 2012, **45**, 8013-8020.

(57) Y. Sageshima, S. Arai, A. Noro and Y. Matsushita, Langmuir 2012, **28**, 17524-17529.

(58) S. Kuo, C. Wu and F. Chang, Macromolecules 2003, **37**, 192-200.

(59) R. Ho, T. Lin, M. Jhong, T. Chung, B. Ko and Y. Chen, Macromolecules 2005, **38**, 8607-8610.

Table of Contents

An ABA triblock containing a central soft block of poly[2,5-di(*n*-hexogycarbonyl)styrene]and outer hard block of poly(4-vinylpyridine): synthesis, phase behavior and mechanical enhancement

Xin Liu,[†] Rui-Ying Zhao,[†] Ti-Peng Zhao,[‡] Chen-Yang Liu,[‡] Shuang Yang[†,] and Er-Qiang Chen[†,*]*

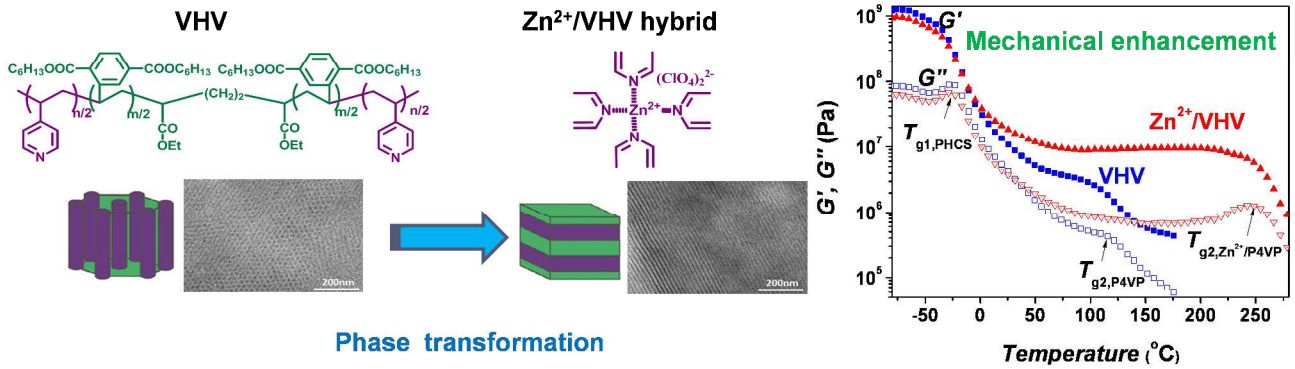

A new ABA triblock copolymer (P4VP-PHCS-P4VP) with strong microphase separation was successfully synthesized and showed phase transformation and mechanical enhancement by blending with metal salt.